Quercetin ameliorates ferroptosis of rat cardiomyocytes via activation of the SIRT1/p53/SLC7A11 signaling pathway to alleviate sepsis-induced cardiomyopathy

XIN LIN*, XIAOXIA ZHAO*, QINGFENG CHEN, XIAOYUE WANG, YONGYA WU and HAO ZHAO

Department of Emergency and Critical Care Medicine, Affiliated Hospital of Shandong University of Traditional Chinese Medicine, Jinan, Shandong 250014, P.R. China

Received April 11, 2023; Accepted September 18, 2023

DOI: 10.3892/ijmm.2023.5319

Abstract. Sepsis-induced cardiomyopathy (SIC) is a manifestation of multiple organ failure as a result of sepsis and is a serious threat to life. Here, the effect and mechanisms of quercetin (QUE) in SIC were assessed. It was found that patients with SIC expressed lower serum levels of glutathione peroxidase 4 (GPX4) and SIRT1 but higher levels of CK-MB, cTnI, TNF-α, and IL-6 compared with healthy individuals. A dose of 80 μM QUE increased the viability and reduced the ferroptosis of H9C2 cells treated with 1.0 μg/ml LPS *in vitro*. The administration of QUE decreased the levels of MDA, NADPH, lipid peroxidation and cytoplasmic cytochrome C and upregulated the levels of GSH and TOM 20, thus exerting an anti-oxidative effect via mediating SIRT1 expression. It also activated the SIRT1/p53/SLC7A11 signaling pathway to reduce cellular Fe^{2+} and PTGS2 levels, decreased cell apoptosis rate, and upregulated the levels of GPX4 and ferritin to inhibit ferroptosis of H9C2 cells *in vitro*. Injection of QUE into rats activated the SIRT1/p53/SLC7A11 signaling pathway, reduced the levels of CK-MB, cTnI, inflammatory cell infiltration, MDA, NADPH, cytoplasmic cytochrome C, cellular Fe^{2+}, and PTGS2 but upregulated the levels of GSH, TOM 20, GPX4, and ferritin to alleviate SIC in a dose-dependent manner *in vivo*. To conclude, QUE exerted an anti-ferroptotic effect via activation of the SIRT1/p53/SLC7A11 signaling pathway to dampen SIC both *in vivo* and *in vitro*. These findings highlighted a potential therapeutic strategy for the management of SIC.

Correspondence to: Dr Hao Zhao, Department of Emergency and Critical Care Medicine, Affiliated Hospital of Shandong University of Traditional Chinese Medicine, 42 Wenhuaxi Road, Lixia, Jinan, Shandong 250014, P.R. China
E-mail: zhaohaodekeyan@163.com

*Contributed equally

Key words: quercetin, ferroptosis, cardiomyocytes, SIRT1/p53/SLC7A11 signaling pathway, sepsis-induced cardiomyopathy

Introduction

Sepsis is defined as a syndrome of the systemic inflammatory response caused primarily by infection. Sepsis-induced cardiomyopathy (SIC) caused by sepsis is one of the manifestations of multiple organ failure in sepsis. The primary manifestations are myocardial inflammation, ventricular dilation, reduced contractility and impaired ventricular response (1). Myocardial injury due to sepsis is recognized as a serious global health problem, and it is a significant cause of morbidity and mortality (2). Potential mechanisms of SIC include myocardial cell inflammation, programmed cell death such as apoptosis, pyroptosis (3), ferroptosis (4), metabolic changes, autophagy disturbances, and mitochondrial dysfunction (5). Several recent papers have shown that sepsis can induce ferroptosis in cardiomyocytes (6-8), and thus causes cardiomyopathy and dysfunction. Therefore, identifying a therapeutic agent to improve myocardial injury in patients with sepsis may provide an important reference to reduce the mortality of patients.

Ferroptosis is an iron-dependent means of programmed cell death. It is a type of regulated cell death that is induced by a combination of iron toxicity, lipid peroxidation, and plasma membrane damage. Ferrous iron or lipoxygenase catalyzes liposome peroxidation of highly expressed unsaturated fatty acids present at the cell membrane to induce cell death (9); its primary feature is decreased levels of glutathione (GSH) and glutathione peroxidase 4 (GPX4) (10). Two GSH molecules serve as electron donors to diminish phospholipid peroxide (PL-OOH) to the corresponding alcohol under the action of GPX4 and generate oxidized glutathione (GSSG) at the same time; GSSG can be reduced by glutathione. The enzyme GSR utilizes NADPH to reduce GSH, forming a cycle. Without deoxidation of peroxidative toxicity by reduction to the corresponding alcohol via GPX4 action, di/trioxycephalin [OO(O)-AA/AdA-PE) accumulates and propagates lipid peroxidation to other phospholipids, eventually leading to impaired membrane integrity and iron death. On the one hand, cell ferroptosis is often accompanied by GSH depletion, decreased GPX4 activity, lipid peroxides that cannot be metabolized by the GPX4-catalyzed reduction reaction, and lipids are oxidized by ferrous iron in a Fenton

reaction, producing ROS and damaging the mitochondria, thereby further promoting the occurrence of ferroptosis and inflammation (11). On the other hand, ferroptosis can affect inflammation through its immunogenicity by release of DAMPs or promoted COX and lipoxygenase activity through the release of oxidized lipid mediators to trigger inflammation (9). Thus, identifying special pathogenic mechanisms may contribute to the development of a therapeutic strategy for myocardial recovery in patients with sepsis.

A previous study showed that the treatment of rat cardiomyocyte cell line H9C2 with 1 μg/ml LPS for 24 h as a model of sepsis *in vitro* can induce ferroptosis in H9C2 cells (7). In addition, there is evidence that in H9C2 cells treated with LPS, the SIRT1/p53/SLC7A11 pathway is inhibited by LPS and causes inflammation and ferroptosis (12). The SIRT1/p53/SLC7A11 pathway is an important regulatory pathway for ferroptosis (13), and studies have shown that activating this pathway by expressing the USP22 protein can slow ferroptosis in H9C2 cells (12). SIRT1 has also been reported to stimulate antioxidant-related protein expression, repair cells damaged by oxidative stress, and prevent cell dysfunction. The reduced SIRT 1 level leads to mitochondrial dysfunction by increasing ROS levels, lipid peroxidation, and DNA damage (14). Therefore, the involvement of SIRT1 and its downstream signaling pathways ensured its unique roles in the progression of SIC.

Quercetin (QUE) is a dietary flavonoid widely present in the plant kingdom with oxidative stress-regulating and anti-inflammatory functions (15). In LPS-induced kidney injury, QUE can exert anti-inflammatory and anti-oxidant effects by increasing SIRT1 expression and inhibiting NF-κB signaling (16). In diabetic encephalopathy, QUE can exert anti-inflammatory effects by increasing the expression of SIRT1 and inhibiting the expression of NLRP3 (17). In suppressing cellular ferroptosis, QUE can alleviate the ferroptosis of hepatocytes by protecting mitochondria and reducing ROS (18). Similarly, QUE can inhibit oxidative stress and ROS production in acute kidney injury, and reduce inflammation and ferroptosis in rat renal tubular duct epithelial cells (19). It has also been shown that in rat cardiomyocytes H9C2, QUE protects cardiomyocytes from hypoxia/reoxygenation-induced apoptosis by modulating the ERK pathway, reducing oxidative stress and mitochondrial damage (20).

Therefore, in the present study, the effects of QUE and its underlying mechanisms in SIC were assessed to provide a potential therapeutic option for the management of SIC.

Materials and methods

Patients. The present study was approved by the Ethics Committee of the Affiliated Hospital of Shandong University of Traditional Chinese Medicine and was performed in accordance with the Declaration of Helsinki. A total of 20 healthy donors (male, 11; female, 9) with a mean age of 48.7±15.3 and 20 SIC patients (male, 10; female, 10) aged 46.2±15.9 were enrolled in this study and written informed consent was obtained. No significance was observed between the healthy donors and the SIC patients concerning sex and age. The inclusion criteria were: Patients were diagnosed with sepsis according to the American College of Chest Physicians/Society of Critical Care Medicine (ACCP/SCCM) (21). Individuals with a history of any heart diseases and cardiac surgery, autoimmune diseases, malignant tumors, or exposure to toxic drugs were excluded. From patients, 5 ml elbow venous blood was collected, and the serum was obtained via centrifugation at 1,000 x g for 10 min at room temperature. The serum levels of GPX4 (cat. no. ab282257), SIRT1 (cat. no. ab171573), CK-MB (cat. no. ab193696), cTnI (cat. no. ab200016), TNF-α (cat. no. ab181421), and IL-6 (cat. no. ab281515) (all from Abcam) levels were measured using commercial ELISA kits and a VersaMax microplate reader.

Cell culture. H9C2 myofibroblasts were purchased (Procell) and cultured in DMEM containing 10% FBS and 1% antibiotics penicillin/streptomycin (Procell Life Science & Technology Co., Ltd.) in an incubator with 5% CO_2 and 95% air (v/v) at 37˚C. To establish the SIC cell model, the H9C2 cells were treated with LPS (0.5, 1.0, 1.5, and 2.0 μg/ml; Beijing Solarbio Science & Technology Co., Ltd.) for 24 h. To determine the appropriate concentration of QUE, different concentrations of QUE (20, 40, 80, and 160 μM) (MedChemExpress) and 1.0 μg/ml LPS were applied to the cell culture for 24 h. The levels of GSH, MDA, NADPH, and intracellular Fe^{2+} were measured using commercial kits (Beyotime Institute of Biotechnology) and a VersaMax reader.

Cell transfection. H9C2 cells were plated into six-well plates with the density of $1x10^5$. When cells reached 60-80% confluence, the cells were transiently transfected with 50 nM siRNA-negative control (NC) or siRNA-SIRT1 (siSIRT1) (synthesized by Shanghai GenePharma Co.) by Lipofectamine 2000 (Invitrogen) according to the manufacturer's protocol. The cells were cultivated in an incubator at 37˚C with 5% CO_2 for 18-48 h. The transfection efficiency was verified at 24 h after transfection at mRNA and protein levels. After 48 h transfection, the transfected cells were used for the subsequent experiments. The sequences of siRNA against SIRT1 and the siRNA-negative control were as follows:

siSIRT1, sense: 5'-CCAGUAGCACUAAUUCCAATT-3', antisense: 5'-UUGGAAUUAGUGCCACUGGTT-3')

Negative NC, sense: 5'-UUCUCCGAACGUGUCACG UTT-3', antisense: 5'-ACGUGACACGUUCGGAGAATT-3').

MTT assay. H9C2 cells ($1x10^4$ cells/well) were maintained in 96-well plates. Then, 20 μl MTT (Shanghai Yeasen Biotechnology Co., Ltd.) was added and maintained for 4 h. Then the formazan crystals were dissolved using 150 μl DMSO (Shanghai Yeasen Biotechnology Co., Ltd.). The optical density (OD) value was measured at 490 nm using a VersaMax microplate reader.

Rats. This study was approved by the Laboratory Animal Ethics Committee and followed the Guide for the Care and Use of Laboratory Animals. A total of 32 adult Sprague-Dawley rats (Beijing Fuhao Experimental Animal Breeding Center) were maintained under a 12-h light/dark cycle with access to water and standard chow. The rats were grouped as follows (n=8 per group): Normal, model, model + 20 mg/kg QUE, model + 40 mg/kg QUE. The rats in the normal group were injected with 150 and 150 μl DMSO was

also injected into the rats in the model group 6 h before SIC modeling. The rats in the model + 20 mg/kg QUE and model + 40 mg/kg QUE groups were injected with 150 μl DMSO + 20 or 40 mg/kg QUE dehydrates 6 h before establishing the SIC model. To establish the SIC model, the rats were anesthetized using 3% halothane. After shaving and disinfecting, cecal ligation and puncture (CLP) was performed using a median incision. CLP is referred to as the 'gold standard' rodent model for abdominal sepsis, it creates a continuously leaking, polymicrobial infectious focus in the abdomen. This was performed following the protocol generated by Drechsler and Osuchowski (22). The abdominal cavity of rats was opened, and after exposing the cecum, 1.5 cm of the cecum was ligated with a 3-0 silk thread and punctured twice with an 18-gauge needle, the abdomen was sealed with 5-0 thread. Bacteremia appeared 6 h after CLP and within 12-24 h, the developed clinical signs of a systemic bacterial infection including fever, chills, erect hair, general weakness, and decreased activity were observed in rats after CLP indicating successful establishment of the model. Two investigators monitored the health and behavior of rats every 4 h after CLP. Of the 32 adult Sprague-Dawley rats one died as a result of severe sepsis after CLP, the 31 living rats were used for the subsequent experiments. The serum levels of GPX4 (cat. no. ab243674), SIRT1 (cat. no. ab242725), CK-MB (cat. no. ab285275), and cTnI (cat. no. ab24460) (all from Abcam) were measured 24 h after CLP using commercial kits and a VersaMax microplate reader. A total of 48 h after CLP, according to the results of the murine sepsis score (MSS) scoring protocol the live rats were sacrificed using CO_2 at a volume displacement of 30-70% vol/min in accordance with the AVMA Guidelines for the Euthanasia of Animals. Then the cardiac tissues of the rats were collected for subsequent experiments. The entire animal experiment lasted ~5 months including animal ordering and purchase, feeding, SIC model establishment, and the subsequent detection.

Histology. Heart tissue was fixed with 4% formaldehyde for 18-24 h at room temperature, embedded in paraffin, and sectioned into 5 μm thickness. To detect inflammatory cell infiltration and iron in the tissues, deparaffinized tissue sections were hydrated using ethanol. Subsequently, sections were processed with a hematoxylin and eosin staining kit according to the manufacturer's protocol (Beyotime Institute of Biotechnology) and a Prussian Blue Iron Staining kit (Shanghai Yeasen Biotechnology Co., Ltd.) and observed with a microscope (Olympus BX51) under the brightfield with the magnification of x100 and x400.

Reverse transcription-quantitative PCR. RNA extraction was performed using an RNApure kit (Bioteke Corporation). RT was performed using a Super M-MLV kit (Shanghai Yeasen Biotechnology Co., Ltd.). qPCR was performed using a QuantStudio 7 Pro (Applied Biosystems; Thermo Fisher Scientific, Inc.) using a SYBR MasterMix (Beijing Solarbio Science & Technology Co., Ltd.) and a 2x Power Taq PCR MasterMix (Bioteke Corporation) and the relative changes in gene expression were analyzed using the $2^{-\Delta\Delta Cq}$ method (23). The sequences of primers were as follows: SIRT1 forward, 5'-GAGTGTGCTGGAGGATCTG-3' and reverse, 5'-TGC TCTGATTTGTCTGGTGT-3'; and β-actin forward, 5'-ACC CGCGAGTACAACCTTCT-3' and reverse, 5'-ATGGCTACG TACATGGCTGG-3'.

Western blotting. Proteins were extracted with RIPA Lysis Buffer (Solarbio) and quantified using BCA kit (Beijing Solarbio Science & Technology Co., Ltd.). 20 μg protein was loaded per lane and separated with 10% SDS-PAGE (GenScript) and transferred to PVDF membranes (MilliporeSigma), the primary antibodies used were: Anti-GPX4 (1:1,000, cat. no. ab125066, 22 kDa), anti-PTGS2 (1:1,000, cat. no. ab179800, 69 kDa), anti-ferritin (1:1,000, cat. no. ab75973, 21 kDa), anti-SIRT1 (1:1,000, cat. no. ab110304, 110 kDa), anti-acetyl-p53 (K382) (1:1,000, cat. no. ab75754, 53 kDa), anti-SLC7A11 (1:1,000, cat. no. ab175186, 55 kDa), anti-TOM20 (1:1,000, cat. no. ab186735, 16 kDa), cytoplasmic cytochrome C (1:1,000, cat. no. ab133504, 11 kDa), and β-actin (1:5,000, cat. no., ab6276, 42 kDa) (all from Abcam), and blots were incubated with primary antibody for 4˚C for 12 h, after which membranes were incubated the secondary HRP-conjugated antibody (1:2,000, cat. no. ab6789) for 1 h at room temperature. Signals were visualized using a DAB kit (Beijing Solarbio Science & Technology Co., Ltd.) and processed using ImageJ 1.46R version (National Institutes of Health).

Flow cytometry. A total of $1x10^5$ H9C2 cells were seeded in 6-well plates, treated with QUE for 24 h, digested and resuspended in 150 μl binding buffer, and stained in the dark with Annexin V-FITC/PI staining kit (BD Biosciences) containing 5 μl FITC-conjugated Annexin V and 5 μl PI for 15 min at room temperature. The apoptosis rate of H9C2 cells was obtained using a FACSCalibur flow cytometer (BD Biosciences) and analyzed by FlowJo 10.6.2 (Becton Dickinson & Company).

Lipid peroxidation assay. For this assay, an Image-iT lipid peroxidation assay kit (Thermo Fisher Scientific, Inc.) was used. The cells were treated with 25 μl Image-iT lipid peroxidation sensor and incubated for 0.5 h at 37˚C. The media was removed, and the cells were washed with PBS (Beijing Solarbio Science & Technology Co., Ltd.) and imaged by a fluorescence microscope (Olympus CKX53, Olympus Corporation) with the magnification of x200. The fluorescence was read at two separate wavelengths. Excitation/emission of 581/591 nm for the reduced dye (red), and the other at excitation/emission of 488/510 nm for the oxidized dye (green).

Immunofluorescence analysis. A total of 1 ml precooled 0.9% NaCl buffer was thoroughly homogenized using 50 mg tissue, and after centrifugation with 1,000 x g for 10 min at 4˚C by a low speed freezing centrifuge, 200 μl supernatant was mixed with 2 μl dihydroethidium probe (Beijing Biolab Technology Co., Ltd.) and incubated for 0.5 h at 37˚C. The images were obtained using a fluorescence microscope (Ex/Em=535/610 nm; Olympus CKX53, Olympus Corporation).

Statistical analysis. The experiments were performed in triplicate and repeated three times. Data are presented as the mean ± SEM. GraphPad Prism version 9.3.3 (GraphPad Software, Inc.) was used for analysis. Pearson's correlation test was used for correlation analysis. Statistical significance was

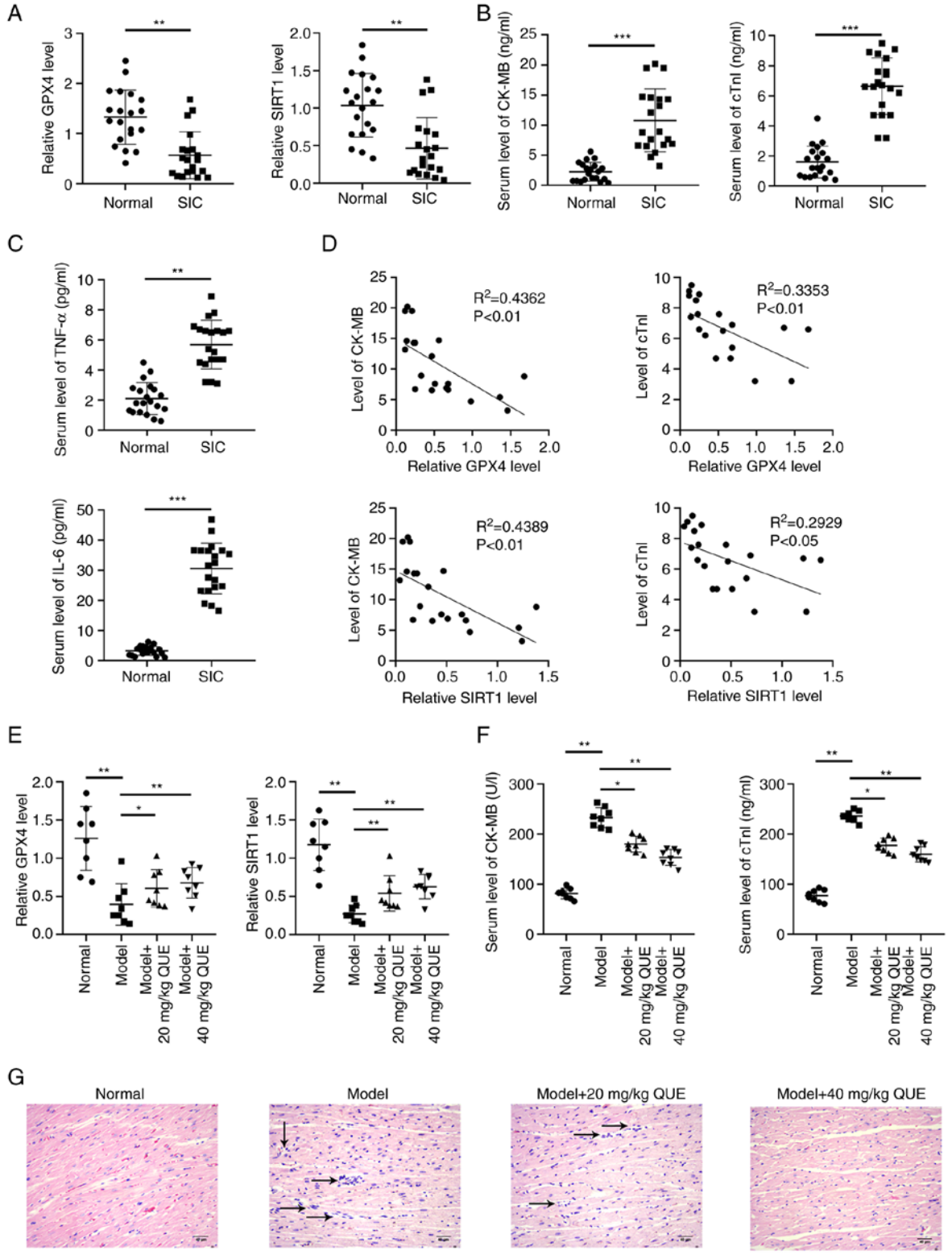

Figure 1. Measurement of the serum levels of GPX4, SIRT1, markers of cardiac injury, and markers of the oxidative stress responses in the clinical samples and rat SIC models. Serum levels of (A) GPX-4 and SIRT1, (B) CK-MB and cTnI and (C) TNF-α and IL-6 in SIC patients and healthy donors. (D) Correlation between GPX4, SIRT1, CK-MB, and cTnI in the 20 SIC patients. Serum levels of (E) GPX-4 and SIRT1, and (F) of cardiac injury markers in the rat model of SIC. (G) Inflammatory cell infiltration in the rat cardiac tissues was assessed using hematoxylin and eosin staining. *P<0.05, **P<0.01, ***P<0.001. GPX4, glutathione peroxidase 4; SIC, Sepsis-induced cardiomyopathy.

analyzed using an unpaired Student's t-test between two groups or a one-way ANOVA with Bonferroni post hoc analysis for comparisons between multiple groups. P<0.05 was considered to indicate a statistically significant difference.

Results

GPX4 and SIRT1 and inflammatory oxidative stress marker levels are increased in the serum of SIC patients. To assess

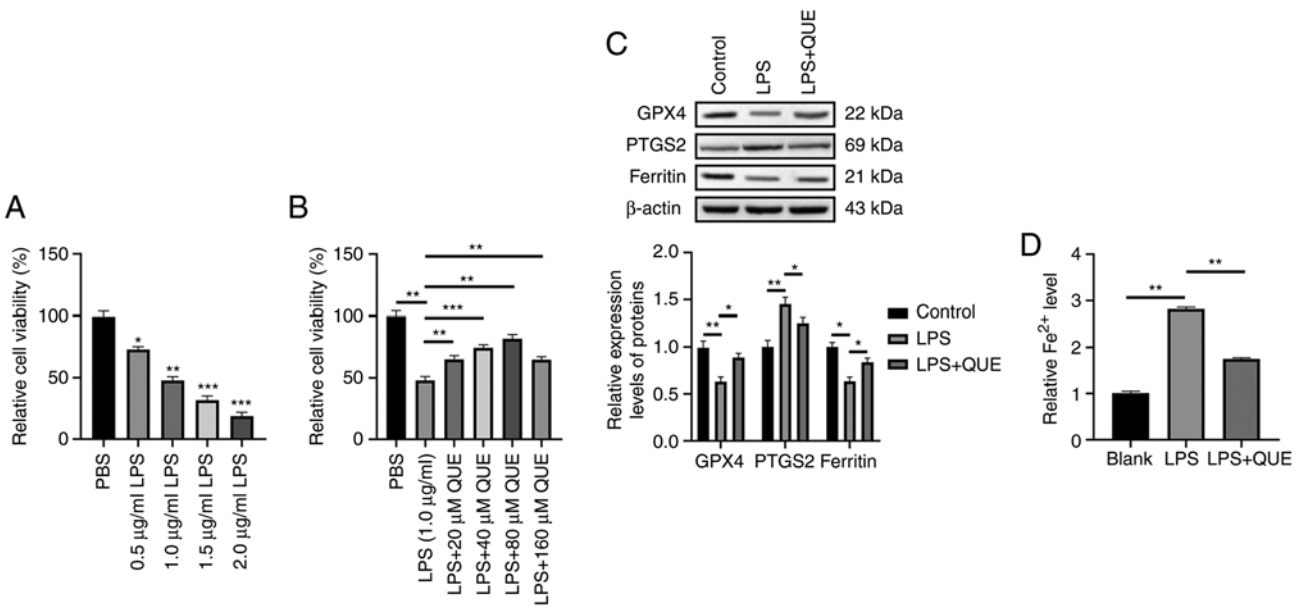

Figure 2. QUE inhibited LPS-induced ferroptosis of H9C2 cells *in vitro*. Viability of H9C2 cells treated with different concentrations of (A) LPS (0.5, 1.0, 1.5, 2.0 μg/ml) for 24 h was determined using an MTT assay. (B) The viability of H9C2 cells treated with QUE (20, 40, 80 and 160 μM) and 1.0 μg/ml LPS for 24 h was determined using MTT assay. (C) The expression levels of ferroptosis-related proteins were detected by western blotting. (D) The levels of Fe^{2+} were measured using a commercial kit. *P<0.05, **P<0.01, ***P<0.001. QUE, quercetin.

the properties of the serum samples of 20 healthy donors and 20 SIC patients, blood samples were collected, and serum was obtained. Next, the serum levels of GPX4, SIRT1, markers of myocardial injury (CK-MB and cTnI), and markers of inflammatory oxidative stress (TNF-α and IL-6) were measured. The results indicated that the serum levels of GPX4 and SIRT1 were lower whereas the levels of myocardial injury and inflammatory oxidative stress markers were higher in the serum of SIC patients compared with the serum of healthy donors (Fig. 1A-C). Using a Pearson's correlation test, serum levels of GPX4 and SIRT1 in 20 SIC patients were negatively correlated with the serum levels of CK-MB and cTnI (Fig. 1D). This indicated that cell ferroptosis was closely associated with SIC.

QUE increases the levels of GPX4 and SIRT1 and decreases the levels of markers of myocardial injury in a dose-dependent manner in vivo. To determine the potential protective effects of QUE against SIC *in vivo*, the rats were divided into four groups (normal, model, model +20 mg/kg QUE and model +40 mg/kg QUE) and the serum levels of GPX4, SIRT1, and markers of myocardial injury markers were tested. The SIC model group had lower levels of GPX4 and SIRT1 but higher levels of CK-MB and cTnI compared with the normal group. The injection of QUE upregulated the levels of GPX4 and SIRT1 and it showed beneficial effects against cardiac injury caused by sepsis based on the reduction in the levels of CK-MB and cTnI, and this effect was dose-dependent manner, thus reducing SIC (Fig. 1E and F). To investigate the pathology of sepsis in inducing cardiac injury and the mechanism of action of QUE, the rat cardiac tissues were stained using hematoxylin and eosin and it was shown that the number of inflammatory cells increased in the model group and injection of QUE reduced inflammatory cell infiltration in cardiac tissues. When 40 mg/kg QUE was used, a better anti-inflammatory effect was observed than 20 mg/kg QUE (Fig. 1G). These results showed that QUE upregulated the levels of GPX4 and SIRT1 and reduced the levels of markers of myocardial injury in a dose-dependent manner *in vivo*.

QUE inhibits LPS-induced ferroptosis of H9C2 cells in vitro. To explore the roles and molecular mechanism of QUE in treating SIC, the H9C2 cells were treated with different concentrations of LPS (0.5, 1.0, 1.5, or 2.0 μg/ml) for 24 h and the results of the MTT assay showed that the viability of H9C2 cells decreased in a dose-dependent manner and the viability of cells treated with 1.0 μg/ml LPS was ~50% of the viability of cells treated with PBS (Fig. 2A). Thus, 1.0 μg/ml LPS was selected for the establishment of the *in vitro* model of SIC. Next, different concentrations of QUE (20, 40, 80, and 160 μM) and 1.0 μg/ml LPS to treat the H9C2 cells for 24 h. It was found that the cell viability was elevated when the concentration of QUE increased, but the viability was reduced when the concentration of QUE was 160 μM. In the LPS + 80 μM QUE group, the cell viability was ~80% of the viability of cells in the PBS group (Fig. 2B). Therefore, 80 μM QUE was used for the subsequent experiments.

The anti-ferroptotic effect of QUE was examined using western blotting and commercial kits, and it was found that 1.0 μg/ml LPS treatment increased the levels of PTGS2 and intracellular Fe^{2+} and reduced the expression of GPX4 and ferritin. QUE decreased the levels of PTGS2 and intracellular Fe^{2+} and increased the expression of GPX4 and ferritin (Fig. 2C and D). These results illustrated that QUE ameliorated ferroptosis of H9C2 cells induced by 1.0 μg/ml LPS.

QUE suppresses LPS-induced oxidative stress by mediating SIRT1 expression in H9C2 cells in vitro. Since it was found that QUE could increase the expression levels of SIRT1 *in vivo* in Fig. 1E and both QUE (24) and SIRT1 (14) have been reported to exert anti-oxidative roles; thus, whether QUE

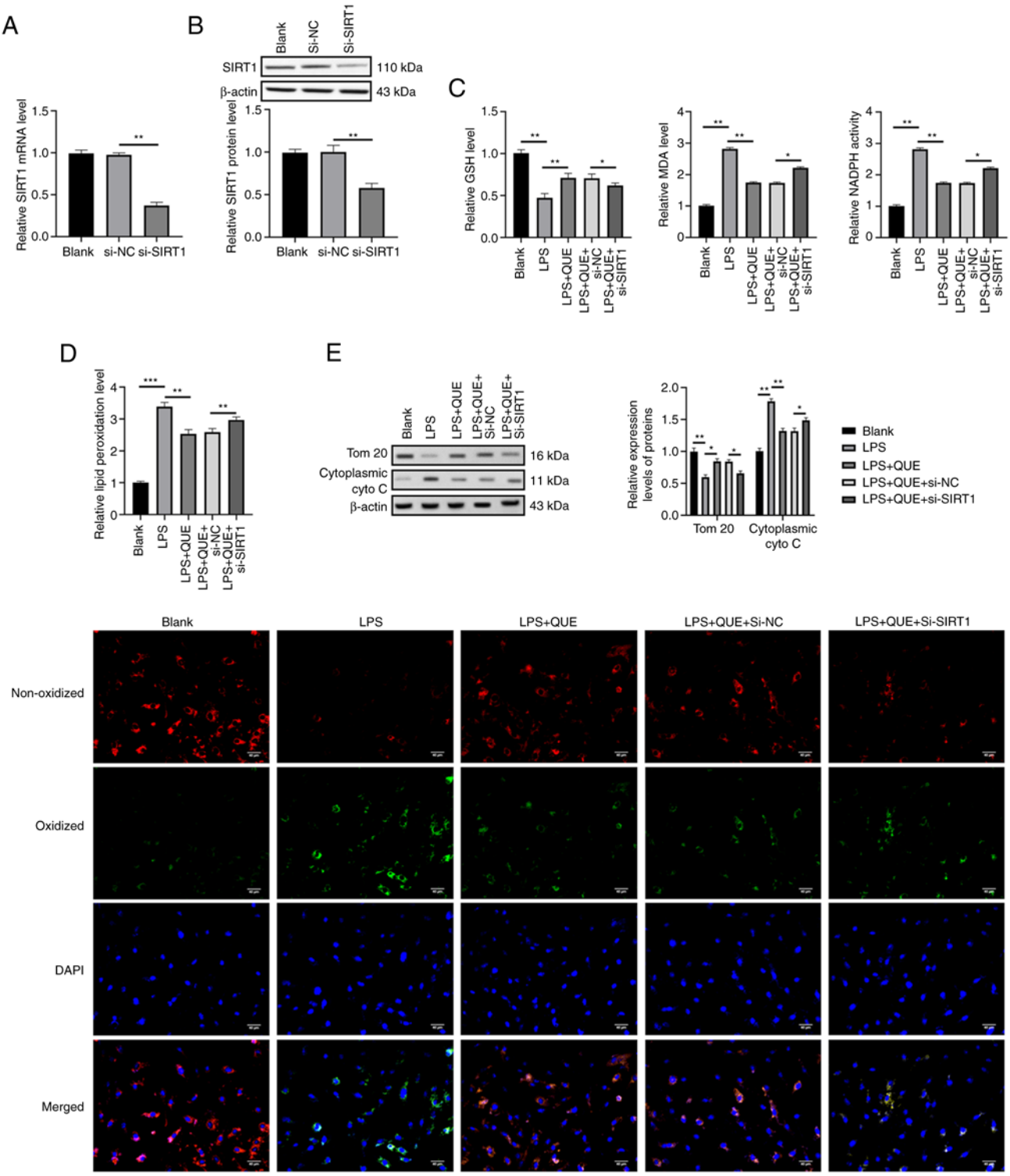

Figure 3. QUE suppressed LPS-induced oxidative stress by mediating SIRT1 expression in H9C2 cells *in vitro*. (A and B) siRNA mediated knockdown of SIRT1 was confirmed at the mRNA and protein level. (C) The levels of oxidative stress response markers were examined using commercial kits. (D) The levels of lipid peroxidation were measured by immunofluorescent assay. (E) The expression levels of mitochondrial-related proteins were detected using western blotting. *P<0.05, **P<0.01, ***P<0.001. QUE, quercetin; siRNA, small interfering RNA; NC, negative control.

played anti-oxidative roles via modulating SIRT1 expression in the *in vitro* SIC cell model was investigated. siRNA against SIRT1 was transfected into H9C2 cells to knock down endogenous SIRT1 expression and the transfection efficiency was confirmed (Fig. 3A and B). Next, the levels of oxidative stress response markers (GSH, MDA, NADPH, and lipid peroxidation) in H9C2 cells were measured using ELISA and immunofluorescent microscopy. The results showed that the LPS group exhibited higher levels of MDA, NADPH, and lipid peroxidation but a lower level of GSH compared with the blank group. QUE reduced the oxidative stress response of cells by increasing the GSH levels and decreasing the MDA, NADPH, and ROS levels. Additionally, knockdown of SIRT1 partially counteracted the anti-oxidative effects of QUE by increasing

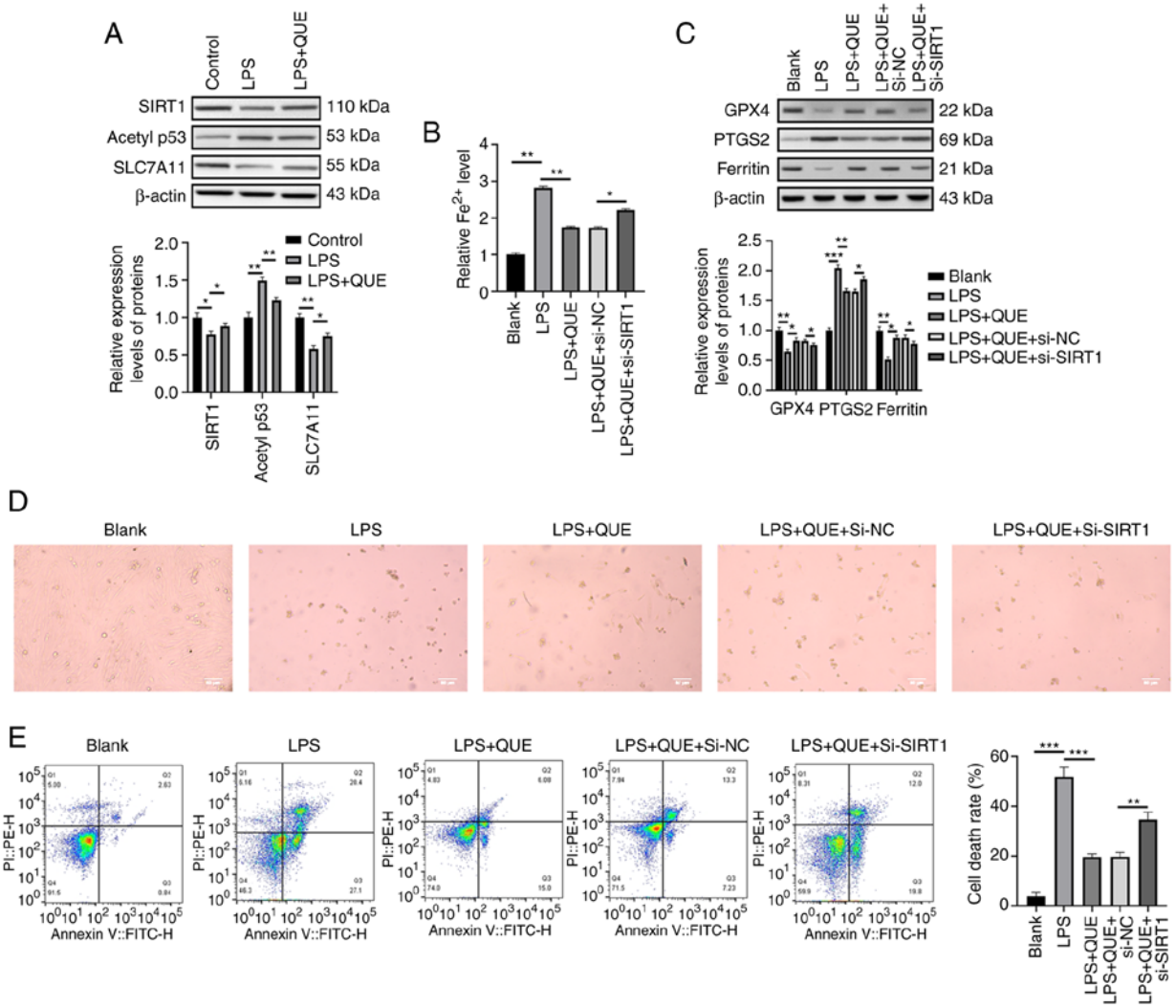

Figure 4. QUE activated the SIRT1/p53/SLC7A11 signaling pathway to inhibit ferroptosis of H9C2 cells *in vitro*. (A) The expression levels of the SIRT1/p53/SLC7A11 pathway-associated proteins were detected by western blotting. (B) The levels of Fe^{2+} were evaluated using a commercial kit. (C) The expression levels of ferroptosis-related proteins were detected by western blotting. (D) Death of H9C2 cells under different treatment conditions. (E) Cell death rate was detected by flow cytometry. *P<0.05, **P<0.01, ***P<0.001. QUE, quercetin; si, small interfering; NC, negative control.

the levels of MDA, NADPH and lipid peroxidation and reducing the levels of GSH (Fig. 3C and D). Given the highly activated oxidative stress response was associated with mitochondrial injury, the expression levels of mitochondrial proteins were evaluated by western blotting. The cells in the LPS group exhibited a higher level of cytoplasmic cytochrome C and a lower level of TOM 20 compared with the blank group, which indicated that LPS treatment induced mitochondrial damage. The damaging effects of LPS were neutralized by QUE via increasing the expression of TOM 20 and downregulating cytoplasmic cytochrome C levels. Compared with the LPS + QUE +si-NC group, the protective roles of QUE on mitochondria were then reversed by si-SIRT1 in the LPS+QUE+si-SIRT1 group (Fig. 3E). This showed that LPS damaged the mitochondria of H9C2 cells and QUE exerted a protective effect against LPS-induced oxidative-related damages, but the antioxidant impact of QUE was neutralized by the knockdown of SIRT1.

QUE activates the SIRT1/p53/SLC7A11 signaling pathway to inhibit ferroptosis of H9C2 cells in vitro. As it was found that QUE exhibited anti-ferroptotic and anti-oxidative effects on LPS-treated H9C2 cells, to explore its underlying mechanism of action and the involvement of downstream signaling pathways, western blotting was used and it was found that LPS downregulated the expression of SIRT1 and SCL7A11 but upregulated the acetylated levels of p53. QUE suppressed the effect of LPS (Fig. 4A). Next, the ferroptosis of H9C2 cells was determined based on the levels of ferroptosis markers via ELISA and western blotting to verify the suppressive mechanism of QUE against cell ferroptosis. QUE exerted an anti-ferroptotic effect by increasing the intracellular Fe^{2+} levels as well as the expression levels of GPX4 and ferritin and suppressing the expression levels of PTGS2 in the LPS-induced ferroptosis of H9C2 cells. However, its influence was partially reversed by the knockdown of SIRT1 in the LPS+QUE+si-SIRT1 group compared to the LPS +QUE +si-NC group (Fig. 4B and C). Subsequently, the death of H9C2 cells was observed by microscopy and analyzed via flow cytometry. It was found that the cells in the LPS group showed a higher rate of apoptosis, and the administration of QUE reduced this cell death. Knockdown of SIRT1 in the LPS+ QUE+si-SIRT1 group increased the apoptosis of cells in contrast to the LPS + QUE + si-NC group

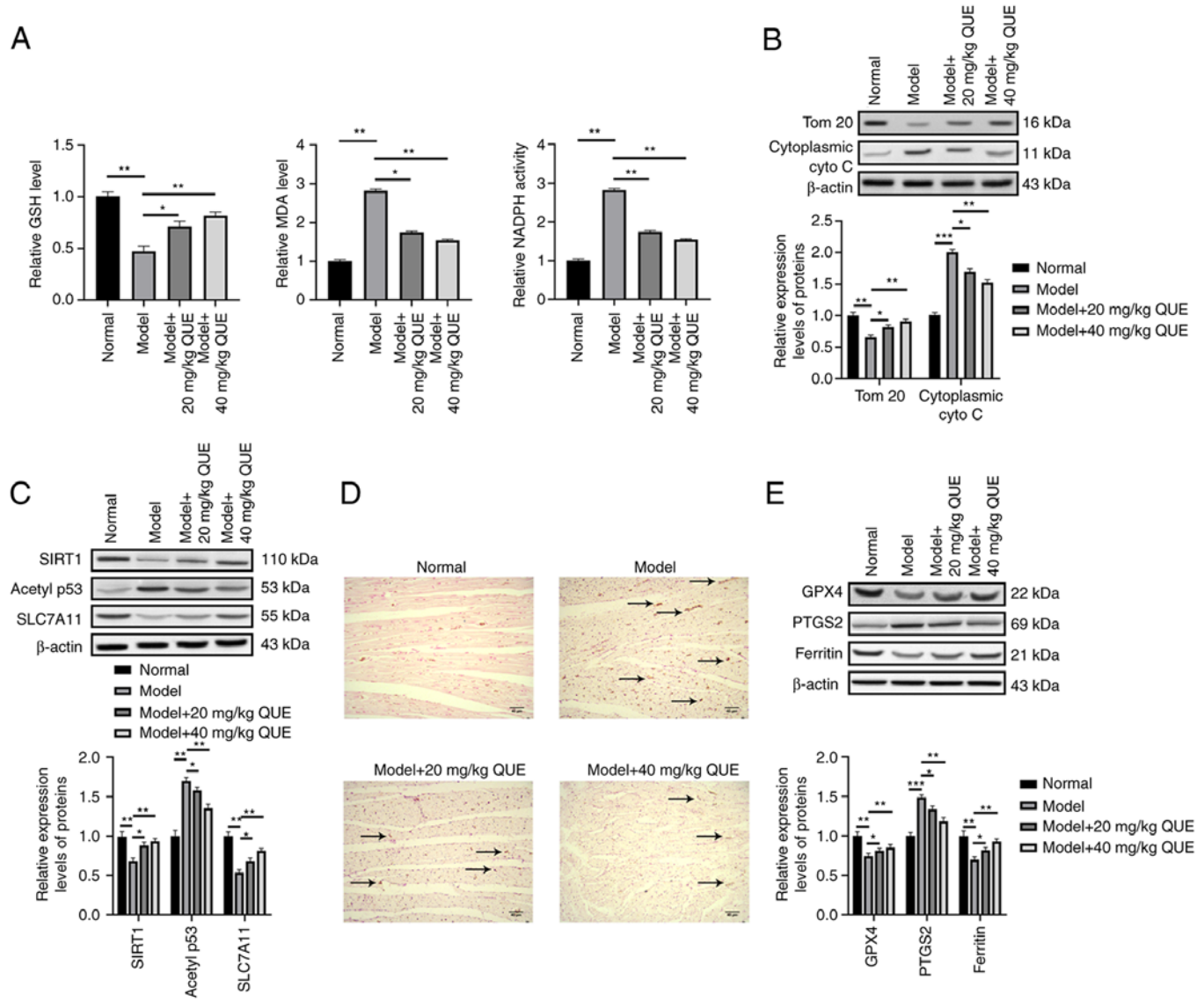

Figure 5. QUE activates the SIRT1/p53/SLC7A11 signaling pathway to inhibit SIC in rats *in vivo*. (A) The levels of oxidative stress response markers were examined using commercial kits. (B) The expression levels of mitochondrial-related proteins were detected by western blotting. (C) Expression levels of pathway-related proteins were detected by western blotting. (D) The deposition of ferric iron was observed using Prussian blue staining. (E) The expression levels of ferroptosis-related proteins were detected by western blotting. *P<0.05, **P<0.01, ***P<0.001. QUE, quercetin.

(Fig. 4D and E). These results revealed that QUE inhibited LPS-induced ferroptosis of H9C2 cells by activating the SIRT1/p53/SLC7A11 signaling *in vitro*.

QUE activates the SIRT1/p53/SLC7A11 signaling pathway to inhibit ferroptosis in vivo. Since the protective effects of QUE in rat models against SIC were determined, next, the molecular mechanism of action was subsequently investigated *in vivo*. First, the levels of oxidative stress response markers (GSH, MDA, and NADPH) in the rat cardiac tissues were measured using commercial ELISA kits to investigate the anti-oxidative effects of QUE. The results showed that the model group exhibited higher levels of MDA and NADPH but lower levels of GSH compared with the normal group. The application of QUE reduced the oxidative stress response in a dose-dependent manner by increasing GSH levels and reducing MDA and NADPH levels (Fig. 5A). Next, to explore the impact of QUE on mitochondria, which are the primary cell organelles responsible for oxidative stress responses, the expression levels of mitochondrial proteins in cardiac tissues were evaluated due to the close relationships between oxidative stress response and mitochondrial injury. The cardiac tissues in the model group expressed higher levels of cytoplasmic cytochrome C and a lower level of TOM 20 compared with the blank group, suggesting the occurrence of mitochondrial damage; and this mitochondrial injury was alleviated by QUE in a dose-dependent manner by increasing the expression of TOM 20 and downregulating cytoplasmic cytochrome C expression (Fig. 5B). This showed that SIC damaged the mitochondria and QUE exerted a mitochondrial protective and anti-oxidative effect against sepsis.

Next, the expression levels of SIRT1, acetyl-p53 (K382), and SLC7A11 in the rat cardiac tissues were detected to investigate the mechanism of action of QUE. The results showed that the rats in the model group exhibited a lower level of SIRT1 and SCL7A11 and a higher level of acetyl-p53. The

injection of QUE-activated SIRT1/p53/SLC7A11 signaling by upregulating the expression of SIRT1 and SCL7A11 and decreasing acetyl-p53 levels, and 40 mg/kg QUE exhibited a more potent effect than 20 mg/kg QUE (Fig. 5C). Finally, the levels of ferroptosis markers in the cardiac tissues were assessed using Prussian blue staining and western blotting to verify the anti-ferroptotic roles of QUE *in vivo*. The Prussian blue staining showed that LPS increased the levels of ferric iron deposition, while its effects were mitigated by QUE in a dose-dependent manner, suggesting that the Fenton reaction could be suppressed by QUE (Fig. 5D). The results of western blotting also confirmed that the model group exhibited a higher level of PTGS2 but lower levels of GSH and ferritin. QUE ameliorated the ferroptosis by reducing PTGS2 and increasing GSH and ferritin expression (Fig. 5E). These results showed that QUE inhibited oxidative stress responses and also weakened cell ferroptosis by activating the SIRT1/p53/SLC7A11 signaling pathway to ameliorate SIC in rats *in vivo*.

Discussion

In the present study, the roles of QUE in SIC were investigated both *in vitro* and *in vivo*. QUE exerted anti-ferroptotic roles via activation of the SIRT1/p53/SLC7A11 pathway to protect mitochondria, reduce oxidative stress response, and relieve SIC. These outcomes corroborated that QUE exhibited potential therapeutic effects in SIC.

Clinically, sepsis-induced a complex myocardial inflammatory response that resulted in myocardial dysfunction. Sepsis can develop into septic shock or multiple organ dysfunction if it is not controlled in a timely and effective manner (25). Despite advances in the understanding of myocardial inflammatory responses, there are no reliable targets and drugs to treat SIC (26). In the present study, administration of LPS to H9C2 cells could induce SIC, stimulate oxidative stress responses, and also induce cell ferroptosis which was consistent with a study by Li *et al* (7). The execution of CLP in rats may lead to tissue inflammation of rats to mimic SIC *in vivo*, which was similar to a previous study (27).

Studies have shown that H9C2 cells undergo ferroptosis due to various reasons such as ischemia/reperfusion injury (28), chemotherapeutic agents (29), and sepsis (30). Ferroptosis is a type of iron-related programmed cell death that differs from apoptosis, necrosis, autophagy, and pyroptosis, and pharmacologically, this cell death process can be inhibited by iron chelators and lipid peroxidation inhibitors (31). Following LPS-triggered ferroptosis of H9C2 cells, the cell viability was decreased, the mitochondria were damaged, and the oxidative stress response was activated. Additionally, the levels of GPX4, which protects cells from ferroptosis, were downregulated. Conditions that lead to GSH exhaustion directly affect the activity and stability of GPX4, thereby making cells more susceptible to ferroptosis (30). Additionally, ferric iron deposition and inflammatory cell infiltration in the cardiac tissues of the experimental sepsis rat model were observed similar to that observed by Li *et al* (7).

Activation of the SIRT1/p53/SLC7A11 signaling pathway is associated with ferroptosis. SIRT1 is an NAD+-dependent deacetylase that directly deacetylates p53 and mediates its pro-apoptotic function (32). SIRT1 functions in catalyzing histone deacetylation and has broad effects on several processes such as anti-inflammation, aging, anti-oxidation, mitochondrial biogenesis, cellular senescence, apoptosis, and circadian rhythms (33). It has been reported that depletion of SIRT1 exacerbates I/R injury (34) and reducing SIRT1 expression protected mice from alcohol-induced liver damage by reducing ferroptosis of hepatocytes (35). In addition, p53 positively regulated cell ferroptosis by inhibiting the expression of SLC7A11, thereby promoting the production of reactive oxygen species (13). Upregulated SLC7A11 expression may inhibit ROS-induced ferroptosis (36). Therefore, these findings suggest that p53/SLC7A11 potentially mediates ferroptosis in cardiomyocytes downstream of SIRT1. To show that QUE reduced cell ferroptosis by increasing SIRT1 expression, *in vitro* experiments were performed by knocking down SIRT1 after the application of QUE, and the results showed that QUE could activate SIRT1/p53/SLC7A11 axis to ameliorate ferroptosis of H9C2 cells and relieve SIC, consistent a study by Ma *et al* (12). However, whether SIRT1 regulated the ferroptosis of cardiomyocytes by deacetylation of P53 remains to be determined. Additionally, to further confirm the results of the present study, the dose of LPS (0.5, 1.0, 1.5, or 2) for the establishment of the *in vitro* model should be increased using a broader range (using concentration in orders of magnitudes) as performed previously (37,38). Additionally, a ferroptosis inducer group should also be included as a positive control of LPS in cell modeling to improve the rigor of the design process. These are the limitations of the present which will be taken into consideration in future studies on the study of QUE, specifically when determining the mechanism of myocardial injury induced by sepsis.

In conclusion, QUE had protective effects on mitochondria and oxidative stress responses and an anti-ferroptotic effect on rat H9C2 cells *in vitro* and a rat model of SIC *in vivo* by stimulating the SIRT1/p53/SLC7A11 pathway. Due to the proinflammatory effect of SIC and the close relationship between ferroptosis and inflammation, the roles of QUE on LPS-induced pyroptosis in SIC using H9C2 cells and a rat model highlighted its potential therapeutic value and its potential mechanism, of action in the management of SIC.

Acknowledgements

Not applicable.

Funding

No funding was received.

Availability of data and materials

The datasets used and/or analyzed during the present study are available from the corresponding author upon reasonable request.

Authors' contributions

XL, YW and HZ conceived and designed the study. XZ, QC, and XW prepared the materials, and acquired and analyzed the data. XL and YW drafted the manuscript. All authors revised the manuscript. All authors have read and approved the final manuscript.

Ethics approval and consent to participate

This study was performed in line with the principles of the Declaration of Helsinki. The present study was approved by the Ethics Committee of the Affiliated Hospital of Shandong University of Traditional Chinese Medicine (approval no. AF/SC-08/02.0). The animal experiments were reviewed and approved by The Institutional Animal Care and Use Committee of the Affiliated Hospital of Shandong University of Traditional Chinese Medicine (approval no. MDL2022-06-15-01). Written informed consent was obtained from all the patients.

Patient consent for publication

Informed consent was obtained for publication of the patient data and images.

Competing interests

The authors declare that they have no competing interests.

References

1. Walley KR: Sepsis-induced myocardial dysfunction. Curr Opin Crit Care 24: 292-299, 2018.
2. Angus DC, Linde-Zwirble WT, Lidicker J, Clermont G, Carcillo J and Pinsky MR: Epidemiology of severe sepsis in the United States: Analysis of incidence, outcome, and associated costs of care. Crit Care Med 29: 1303-1310, 2001.
3. Li N, Zhou H, Wu H, Wu Q, Duan M, Deng W and Tang Q: STING-IRF3 contributes to lipopolysaccharide-induced cardiac dysfunction, inflammation, apoptosis and pyroptosis by activating NLRP3. Redox Biol 24: 101215, 2019.
4. Chen Z, Cao Z, Gui F, Zhang M, Wu X, Peng H, Yu B, Li W, Ai F and Zhang J: TMEM43 protects against sepsis-induced cardiac injury via inhibiting ferroptosis in mice. Cells 11: 2992, 2022.
5. Flierl MA, Rittirsch D, Huber-Lang MS, Sarma JV and Ward PA: Molecular events in the cardiomyopathy of sepsis. Mol Med 14: 327-336, 2008.
6. Kong C, Ni X, Wang Y, Zhang A, Zhang Y, Lin F, Li S, Lv Y, Zhu J, Yao X, *et al*: ICA69 aggravates ferroptosis causing septic cardiac dysfunction via STING trafficking. Cell Death Discov 8: 187, 2022.
7. Li N, Wang W, Zhou H, Wu Q, Duan M, Liu C, Wu H, Deng W, Shen D and Tang Q: Ferritinophagy-mediated ferroptosis is involved in sepsis-induced cardiac injury. Free Radic Biol Med 160: 303-318, 2020.
8. Zhou B, Zhang J, Chen Y, Liu Y, Tang X, Xia P, Yu P and Yu S: Puerarin protects against sepsis-induced myocardial injury through AMPK-mediated ferroptosis signaling. Aging 14: 3617-3632, 2022.
9. Sun Y, Chen P, Zhai B, Zhang M, Xiang Y, Fang J, Xu S, Gao Y, Chen X, Sui X and Li G: The emerging role of ferroptosis in inflammation. Biomed Pharmacother 127: 110108, 2020.
10. Zhao X and Chen F: Propofol induces the ferroptosis of colorectal cancer cells by downregulating STAT3 expression. Oncol Lett 22: 767, 2021.
11. Ursini F and Maiorino M: Lipid peroxidation and ferroptosis: The role of GSH and GPx4. Free Radic Biol Med 152: 175-185, 2020.
12. Ma S, Sun L, Wu W, Wu J, Sun Z and Ren J: USP22 protects against myocardial ischemia-reperfusion injury via the SIRT1-p53/SLC7A11-dependent inhibition of ferroptosis-induced cardiomyocyte death. Front Physiol 11: 551318, 2020.
13. Xie Y, Hou W, Song X, Yu Y, Huang J, Sun X, Kang R and Tang D: Ferroptosis: Process and function. Cell Death Differ 23: 369-379, 2016.
14. Alam F, Syed H, Amjad S, Baig M, Khan TA and Rehman R: Interplay between oxidative stress, SIRT1, reproductive and metabolic functions. Curr Res Physiol 4: 119-124, 2021.
15. Karimi A, Naeini F, Azar VA, Hasanzadeh M, Ostadrahimi A, Niazkar HR, Mobasseri M and Tutunchi H: A comprehensive systematic review of the therapeutic effects and mechanisms of action of quercetin in sepsis. Phytomedicine 86: 153567, 2021.
16. Lu S, Zhou S, Chen J, Zheng J, Ren J, Qi P, Zhu Z and Li Z: Quercetin nanoparticle ameliorates lipopolysaccharide-triggered renal inflammatory impairment by regulation of Sirt1/NF-KB pathway. J Biomed Nanotechnol 17: 230-241, 2021.
17. Hu T, Lu XY, Shi JJ, Liu XQ, Chen QB, Wang Q, Chen YB and Zhang SJ: Quercetin protects against diabetic encephalopathy via SIRT1/NLRP3 pathway in db/db mice. J Cell Mol Med 24: 3449-3459, 2020.
18. Jiang JJ, Zhang GF, Zheng JY, Sun JH and Ding SB: Targeting mitochondrial ROS-mediated ferroptosis by quercetin alleviates high-fat diet-induced hepatic lipotoxicity. Front Pharmacol 13: 876550, 2022.
19. Wang Y, Quan F, Cao Q, Lin Y, Yue C, Bi R, Cui X, Yang H, Yang Y, Birnbaumer L, *et al*: Quercetin alleviates acute kidney injury by inhibiting ferroptosis. J Adv Res 28: 231-243, 2021.
20. Li F, Li D, Tang S, Liu J, Yan J, Chen H and Yan X: Quercetin protects H9c2 cardiomyocytes against oxygen-glucose deprivation/reoxygenation-induced oxidative stress and mitochondrial apoptosis by regulating the ERK1/2/DRP1 signaling pathway. Evid Based Complement Alternat Med 2021: 7522175, 2021.
21. Li Y, Lu B, Yu M, Zhai J, Yao Y and Chai Y: Diagnostic value and significance of serum miR-132 combined with miR-223 for sepsis-induced cardiomyopathy. Exp Ther Med 22: 1396, 2021.
22. Drechsler S and Osuchowski M: Cecal ligation and puncture. Methods Mol Biol 2321: 1-8, 2021.
23. Livak KJ and Schmittgen TD: Analysis of relative gene expression data using real-time quantitative PCR and the 2(-Delta Delta C(T)) method. Methods 25: 402-408, 2001.
24. Sato S and Mukai Y: Modulation of chronic inflammation by quercetin: The beneficial effects on obesity. J Inflamm Res 13: 421-431, 2020.
25. Angus DC and van der Poll T: Severe sepsis and septic shock. N Engl J Med 369: 840-851, 2013.
26. Hollenberg SM and Singer M: Pathophysiology of sepsis-induced cardiomyopathy. Nat Rev Cardiol 18: 424-434, 2021.
27. Huang X, Zhang MZ, Liu B, Ma SY, Yin X and Guo LH: Astragaloside IV attenuates polymicrobial sepsis-induced cardiac dysfunction in rats via IKK/NF-κB pathway. Chin J Integr Med 27: 825-831, 2021.
28. Zhang Y, Ren X, Wang Y, Chen D, Jiang L, Li X, Li T, Huo M and Li Q: Targeting ferroptosis by polydopamine nanoparticles protects heart against ischemia/reperfusion injury. ACS Appl Mater Interfaces 13: 53671-53682, 2021.
29. Hou K, Shen J, Yan J, Zhai C, Zhang J, Pan JA, Zhang Y, Jiang Y, Wang Y, Lin RZ, *et al*: Loss of TRIM21 alleviates cardiotoxicity by suppressing ferroptosis induced by the chemotherapeutic agent doxorubicin. EBioMedicine 69: 103456, 2021.
30. Park TJ, Park JH, Lee GS, Lee JY, Shin JH, Kim MW, Kim YS, Kim JY, Oh KJ, Han BS, *et al*: Quantitative proteomic analyses reveal that GPX4 downregulation during myocardial infarction contributes to ferroptosis in cardiomyocytes. Cell Death Dis 10: 835, 2019.
31. Chen D, Eyupoglu IY and Savaskan N: Ferroptosis and cell death analysis by flow cytometry. Methods Mol Biol 1601: 71-77, 2017.
32. Chen H, Lin X, Yi X, Liu X, Yu R, Fan W, Ling Y, Liu Y and Xie W: SIRT1-mediated p53 deacetylation inhibits ferroptosis and alleviates heat stress-induced lung epithelial cells injury. Int J Hyperthermia 39: 977-986, 2022.
33. Liu X, Liu J, Xiao W, Zeng Q, Bo H, Zhu Y, Gong L, He D, Xing X, Li R, *et al*: SIRT1 Regulates N(6) -methyladenosine RNA modification in hepatocarcinogenesis by inducing RANBP2-dependent FTO SUMOylation. Hepatology 72: 2029-2050, 2020.
34. Chun SK, Lee S, Flores-Toro J, U RY, Yang MJ, Go KL, Biel TG, Miney CE, Louis SP, Law BK, *et al*: Loss of sirtuin 1 and mitofusin 2 contributes to enhanced ischemia/reperfusion injury in aged livers. Aging Cell 17: e12761, 2018.
35. Zhou Z, Ye TJ, DeCaro E, Buehler B, Stahl Z, Bonavita G, Daniels M and You M: Intestinal SIRT1 deficiency protects mice from ethanol-induced liver injury by mitigating ferroptosis. Am J Pathol 190: 82-92, 2020.
36. Jiang L, Kon N, Li T, Wang SJ, Su T, Hibshoosh H, Baer R and Gu W: Ferroptosis as a p53-mediated activity during tumour suppression. Nature 520: 57-62, 2015.
37. Meyer D, Telele S, Zelená A, Gillen AJ, Antonucci A, Neubert E, Nißler R, Mann FA, Erpenbeck L, Boghossian AA, *et al*: Transport and programmed release of nanoscale cargo from cells by using NETosis. Nanoscale 12: 9104-9115, 2020.
38. Willis C, Morris JM, Danis V and Gallery EDM: Cytokine production by peripheral blood monocytes during the normal human ovulatory menstrual cycle. Hum Reprod 18: 1173-1178, 2003.